Characterization and stabilization of the downward continuation problem for airborne gravity data

Xiaopeng Li[1], Jianliang Huang[2], Roland Klees[3], René Forsberg[4], Martin Willberg[5], Cornelis Slobbe[3], Cheinway Hwang[6], and Roland Pail[5]

[1]National Geodetic Survey, NOAA, 1315 East-West Highway, Silver Spring, MD 20910, USA (xiaopeng.li@noaa.gov)

[2]Canadian Geodetic Survey, Natural Resources Canada, 588 Booth Street, Ottawa, Ontario, Canada.

[3]Delft University of Technology, Building 23, Stevinweg 1/PO box 5048, 2628 CN Delft, the Netherlands.

[4]DTU Space, National Space Institute, Technical University of Denmark, Elektrovej 327, Denmark

[5]Institute of Astronomical and Physical Geodesy, Technical University of Munich, Arcisstrasse 21, 80333, Munich, Germany.

[6]Department of Civil Engineering, National Yang Ming Chiao Tung University, 1001 University Road, Hsinchu 300, Taiwan.

Abstract

In this study, we compare six commonly used methods for the downward continuation of airborne gravity data. We consider exact and noisy simulated data on grids and along flight trajectories and real data from the GRAV-D airborne campaign. We use simulated respectively real surface gravity data for validation. The methods comprise spherical harmonic analysis, least-squares collocation, residual least-square collocation, radial basis function, the inverse Poisson method and Moritz's analytical downward continuation method. We show that all methods perform similar in terms of surface gravity values. For real data, the downward continued airborne gravity values are used to compute a geoid model using a Stokes-integral-based approach. The quality of the computed geoid model is validated using high-quality GSVS17 GPS-levelling data. We show that the geoid model quality is similar for all methods. However, the least-square collocation approach appears to be more robust and flexible than the other methods provided that the optimal covariance function is found. We recommend it for the downward continuation of GRAV-D data, and other methods for second check.

1. Introduction

The Gravity for the Redefinition of the American Vertical Datum (GRAV-D) project aims to cover the US territory with airborne gravity measurements while extending about 100 km into Canada and Mexico. It is the largest airborne gravimetric campaign ever undertaken in the world. The project is to develop a geoid-based vertical datum at the precision of 2 cm for much of the country. The flight heights range from 4 to 11 km with a nominal height of about 6 km to achieve a minimum spatial resolution of 20 km (GRAV-D Team 2017a). The GRAV-D data need to be reduced onto the Earth's surface or geoid when being combined with terrestrial gravity data by the Stokes method to determine a gravimetric geoid model. This reduction step has been termed as the downward continuation (DC). One intermediate question is: which method is most suitable for the DC of airborne gravity data, in particular the high-altitude GRAV-D data? The answer is not yet evident despite studies and the development of DC methods for many decades.

The DC problem (DCP) is an ill-posed problem (Schwarz 1978; Rummel et al. 1979; Jekeli 1981). Schwarz (1978) summarizes numerical features of the ill-posed problem as follows:

a) The solution does not continuously depend on the given data, i.e. small changes in the data may cause large changes in the solution.
b) The matrices resulting from the discretization of the problem will be ill-conditioned, i.e., the condition numbers will be large enough to severely amplify data noise.
c) The accuracy of the solution does not increase with the grid density, i.e., as the grid size becomes smaller, the solution error will increase in any norm.

As Milbert (1999) stated, one is faced with the "dilemma of downward continuation". If one uses a coarse grid, the geoid omission error may be dominant; if one uses a fine grid, the geoid commission error may be dominant, mainly due to noise amplification during downward continuation. He showed numerically that 1 mGal zero-mean white Gaussian noise may be amplified to 47.5 mGal when downward-continued from an altitude of 4000 m without regularisation.

There have been a long history of studies dealing with DCP of airborne gravity data in the context of (quasi-) geoid modelling (see e.g. Forsberg 1987; Novák and Heck 2002, Novák et al 2003). There are three classical methods for the DC of gravity data: i) inverse Poisson, which solves Poisson's integral equation (see e.g. Heiskanen and Moritz 1967; Vaníček et al. 1996; Martinec 1996); ii) Moritz's analytical DC (1980); and iii) Least-Squares Collocation (LSC) (Moritz 1980; Forsberg 1987; Tscherning 2013). In recent decades, Radial Basis Functions (RBF) have become popular in local (quasi-) geoid modelling, but can also be used straightforwardly for gravity DC (e.g. Schmidt et al., 2007; Klees et al.; 2008, Lieb et al. 2016; Li 2018; Liu et al. 2020). Furthermore the Spherical Harmonic Analysis (SHA) method has been adapted for DC of GRAV-D data (Smith et al. 2013; Holmes, 2016). Recently, the Residual LSC (RLSC) has been developed and applied to GRAV-D data (Willberg et al., 2019; 2020). A question naturally arises: do all these methods perform equally?

This paper characterizes the DCP, assesses stability and equivalence of the six DC methods, and finds suitable DC methods for DC of airborne gravity data. Section 2 reviews the DC methods. Section 3 characterizes the ill-posedness of the DCP. Section 4 discusses stabilization methods for the DCP. Section 5 applies the DC methods to GRAV-D data. Section 6 concludes this study.

2. Overview of DC methods

There are six methods considered in this study. The first one is the spherical harmonic analysis approach currently used at the National Geodetic Survey (Smith et al. 2013). The basic idea is to convert the local data into global data by padding zeros outside of the study area with tapering near the border area to have a gradual transition from non-zero values to zero values. Appendix A1 provides more information about this method.

The second method is Least Squares Collocation (LSC). The standard LSC was originally derived for stationary processes and, later, extended to weakly stationary processes (Darbeheshti and Featherstone 2010). The quality of a LSC solution depends on the correctness of the covariance function. In the context of gravity field modeling, there are many previous studies on how to build covariance functions (e.g., Kaula (1959), Krarup (1969), Moritz (1972), Tscherning and Rapp (1974), Forsberg (1987), and Jekeli (2010)). The covariance function which is most commonly used for airborne gravity data is the one by Forsberg (1987), see Appendix A.2. This study also includes the newly developed Residual Least Squares Collocation method (RLSC) (Wilberg et al. 2019; 2020), see Appendix A.3 for more information.

The fourth method is least-squares Radial Basis Functions (RBF) approximation (see e.g. Schmidt et al. 2007; Klees et al. 2008). This method has become popular in regional gravity field modelling due to the quasi-localizing properties of the RBFs (e.g., Schmidt et al., 2007; Klees et al. 2008; Slobbe 2013; Lieb et al. 2016; Slobbe et al. 2019; Liu et al. 2020). Once an RBF model is determined, it can also be used for downward continuation. The detailed formulation is given in Appendix A.4.

The fifth method is based on Poisson's integral and numerically solves a first-kind integral equation (e.g., Heiskanen and Moritz 1967; Vaníček et al. 1996; Martinec 1996; Milbert 1999; Novák and Heck 2002; Alberts and Klees 2004). Several different regularization strategies of this ill-posed problem can be found in previous studies (see e.g., Alberts and Klees 2004, Jiang et al 2011, Liu et al 2016, Zhao et al 2018). More comprehensive discussions of regularization can be found in, e.g., Xu and Rummel (1994), Kusche and Klees (2002), Kern (2003), and Cai et al (2004). In this study, the integral equation is discretized and solved numerically using the method of Huang (2002). The detailed formulation is given in Appendix A.5.

The sixth method included in this study is the Analytical Downward Continuation (ADC), which was formulated for the Molodensky boundary value problem by Moritz (1980). The detailed formulation is given in Appendix A.6.

3. Characterization of the ill-posed problem

3.1 Amplification of errors

In physical geodesy and geophysics, the Earth's gravity field is split into the normal gravity field of a reference ellipsoid and the anomalous gravity field. The normal gravity field is mathematically derived, and subtracted from the Earth's gravity field to compute the anomalous gravity field, which is then modelled and applied for a broad spectrum of applications. There are two conventional parameters to represent the anomalous field. The first is the gravity anomaly, which can be expressed by the spherical harmonics as follows (Heiskanen and Moritz, sect. 2-23, p115, 1967)

$$\Delta g(r\,,\phi\,,\lambda\,) = \sum_{n=0}^{\infty}\left(\frac{R}{r}\right)^{n+2}\Delta g_n(\phi\,,\lambda\,) \tag{1}$$

The triplet $(r\,,\phi\,,\lambda\,)$ represents spherical coordinates (radius, latitude, longitude); R the radius of the geoid in spherical approximation; and Δg_n are the Laplace surface harmonics. The gravity anomaly is used when the orthometric height is available. That is the case for historical surface gravity data. For airborne gravimetry, the positions of the data points are provided by Global Navigation Satellite Systems, and gravity disturbances are the natural choice:

$$\delta g(r\,,\phi\,,\lambda\,) = \sum_{n=0}^{\infty}\left(\frac{R}{r}\right)^{n+2}\delta g_n(\phi\,,\lambda\,) \tag{2}$$

Let $r = R + HC$, and HC is a constant height, then we can express the gravity disturbance at the constant height of HC into the surface spherical harmonics

$$\delta g(R + HC\,,\phi\,,\lambda\,) = \sum_{n=0}^{\infty}\delta g_n^{HC}(\phi\,,\lambda\,) \tag{3}$$

where

$$\delta g_n^{HC}(\phi\,,\lambda\,) = \left(\frac{R}{R+H}\right)^{n+2} \delta g_n(\phi\,,\lambda\,) \tag{4}$$

or

$$\delta g_n(\phi\,,\lambda\,) = \left(\frac{R+HC}{R}\right)^{n+2} \delta g_n^{HC}(\phi\,,\lambda\,) \tag{5}$$

Substituting Equation (5) into Equation (2), and let $r = R$, we obtain the gravity disturbance on the geoid as

$$\delta g(R\,,\phi\,,\lambda\,) = \sum_{n=0}^{\infty} \left(\frac{R+HC}{R}\right)^{n+2} \delta g_n^{HC}(\phi\,,\lambda\,) \tag{6}$$

It can be seen that the gravity disturbance component of degree n at the height of HC is amplified by a factor of $\left(\frac{R+HC}{R}\right)^{n+2}$ when it is continued downward to the geoid. For $HC = 6$ km and $n = 2{,}160$ (corresponding to the 5' spatial resolution), the amplification factor is about 8. When $n = 10{,}800$ (corresponding to the 1' spatial resolution), the amplification factor is about 26,000. The same amplification factors also applies for the error components rendering DCP unstable. A filtering or regularization method must be used to control noise amplification at the cost of introducing a bias into the signal. An effective DC method makes a tradeoff between noise amplification and bias.

3.2 Case simulation 1: regular grids

3.2.1 Simulation set up

Simulation 1 synthesizes a 1'x1' grid of gravity disturbances from EGM2008 (Pavlis et al. 2012) in an area of 5° x 9° [34° - 39°N; 250° - 259°E] at 6200 m altitude (the mean flight height of the MS05 GRAV-D block over the area of Colorado) as input data (see Figure 1). A second grid is synthesized on the reference ellipsoid and serves as the control dataset to quantify DC errors per method. Two noisy datasets were generated by adding i) zero mean white Gaussian noise with a standard deviation of 1 mGal, and ii) colored AR(1) noise with parameter 0.9 and driven by white Gaussian noise with variance 0.19 mGal^2, which ensures that the noise standard deviation is also 1 mGal. This gives three datasets, which differ in terms of the superimposed noise: noise free, white noise, and colored noise, respectively. Figure 2 shows the Power Spectral Density (PSD) of the two noise processes. It shows that the PSD of the AR(1) noise is stronger than that of the white noise at the frequencies below 0.035[cycles/km].

3.2.2 Inverse Poisson

The Poisson DC has been performed using the three sets of simulated input data with the threshold RMS values at 0.001 mGal and 1.0 mGal. These thresholds represent the accuracy of input data without and with noise, respectively. The iterative solutions are convergent for the noise free case regardless the small grid size of 1' and the large altitude of 6200 m. When the 1 mGal white and colored noise are included, the iterative solutions do not converge with the threshold RMS values of 0.001 mGal when the maximum number of iterations is 1000. The noise level is amplified by a factor of 2 and 3 in magnitude when the maximum iterations are set equal to 100 and 1000, respectively. This reflects the ill-conditioning of the inverse Poisson problem for the chosen set-up. Setting the threshold value to 1.0 mGal makes the solutions convergent leading to an error level which is one magnitude higher than the input noise level. The resulting DC errors from 6200 m to 0 m altitudes are evaluated and shown in Figure 3 with the maximum number of

iterations set to 100. DC errors have been estimated with both the full simulation field shown in Figure 1 and the residual fields with respect to a reference model xGeoid16refA truncated at different degree. xGeoid16refA was developed at NGS, and is a combination of EGM2008 and GOCO05s, complete to degree 2159 with some additional coefficients up to degree 2190 similar to EGM2008.

In the case of noise free input data and a threshold of 0.001 mGal, the DC errors shown as red thick lines are smaller than 1 mGal for the full field DC, and smaller than 0.1 mGal for the residual fields. When a threshold of 1 mGal is set with the noise free input, the errors shown as red dash lines increase to several mGal suggesting that the signal of omission below the level of 1 mGal is significantly amplified in the DC solutions. In the case of white and colored noise input data with the threshold of 0.001 mGal, the noise levels are amplified more than 100 times in the DC results. This suggests that filtering high-frequency noise is essential before the Poisson DC is applied. Otherwise the DC fails. The threshold of 1 mGal with the noise input effectively reduces the DC errors to a few mGal, which still is large. Again it points out the necessity of filtering noisy input data before the Poisson DC (see e.g. Alberts and Klees 2004). It is noticeable that the white noise causes larger DC errors than the colored noise. This can be explained by the fact that the PSD of white noise is much larger than that of the AR(1) noise at higher frequencies (cf. Figure 2). There are a few sharp turning patterns in the error curves when using a 0.001 mGal threshold, which are due to numerical round-off errors.

3.2.3 Moritz's ADC

DC errors for Moritz's ADC have been estimated for the 5th order approximation. The results are shown in Figure 4. In the case of noise free data, the DC errors are at the mGal level. However, in the case of noisy input data, the DC errors are 10 to 100 times larger than the input noise level. Similar to the Inverse Poisson, the white noise causes much larger DC errors than the colored noise. There is not an effective way to control the amplification of noise by the method itself other than truncating the ADC series G_n to a lower order, and a pre-filtering process is necessary before the ADC is applied.

3.2.4 RBF without regularization

We only examine the extreme case, which is DC from 6200 to 0 m, and study the amplification pattern of DC errors. Input data are the gravity disturbance residuals with respect to the reference model, xGeoid16refA, truncated at degree 190. A RBF band-limited to degrees 190 to 2190 is fitted using ordinary least-squares to the noise-free, white-noise and colored-noise datasets, respectively. No regularisation was used. For error-free data, the DC errors range from -5 to 5 mGal with a standard deviation of 1 mGal. Figure 5 shows DC errors for the cases of adding white and colored noises to the input data. The magnitude of DC errors by RBF is significantly lower than those by the Inverse Poisson and Moritz's ADC. Note that even better results can be expected if regularisation is applied.

3.3 Case simulation 2: flight lines and surface points

3.3.1. Simulation set up

Here, the noise free, white noise and colored noise datasets are generated along real flight trajectories from GRAV-D's MS05 campaign (in Colorado). The simulated airborne gravity data are shown in Figure 6.

The flight altitudes range from 5200 to 7900 m. There are data gaps in the survey. The mean value is about 5.7 mGal with a standard deviation of 29.1 mGal. Most of the strong signals are found over mountain ridges. These scattered point data at flight levels are used as the observations for a more realistic simulation case. The ground truth data set comprises gravity disturbances from EGM2008, synthesized at the 31,358 NGS

point surface gravity data. The simulated surface gravity disturbances are plotted along with their topographic heights in Figure 7.

Strong variations of gravity disturbance are visible in the mountainous regions in the west. The eastern part is relatively flat. The mean value is about -6.4 mGal with a standard deviation of 30.9 mGal.

3.3.2 RBF without regularization

The three sets of simulated input data in sub-section 3.3.1 are more realistic than the input datasets in sub-section 3.2.1, and are expected to provide a more realistic estimation of DC errors. Following the same RBF modelling procedure and using the same degree of reference field, DC errors have been estimated both at grid points on the reference ellipsoid and at the surface points. For noise free input data,, DC errors range from -3 to 2 mGal; the standard deviations is 0.1 mGal at both grid and surface points. DC errors for the noisy datasets are shown in Figures 8 and 9. Their levels are higher than the input noise level by a factor of about 700 to 1200. We explain this by a combination of different factors: i) the heterogeneous distribution of data points with a dense sampling along the flight trajectories and larger gaps between neighbored tracks; ii) a sub-optimal RBF network for given dataset, and iii) the lack of regularisation.

4. Stabilization of DCP

4.1 Compression of errors

There are three basic methods to compress the errors of DC: spatial filtering, LSC and the least-squares regularization. The first method spectrally filter out errors in gravity data to stabilize DC (e.g., Jekeli 1981), while the second and third methods compress the errors by regularization (see e.g. Rummel et al. 1979). As an example of spectral filtering, SHA acts as a low-pass filter up to the maximum degree of SHA to avoid the high-degree noise. In this section, we assess the three methods using the same simulated data sets as in Section 3.

4.2 Case simulation 1: regular grids

4.1.1. LSC

The first step of LSC is building the covariance functions. Figure 10 shows the empirical covariance functions as well as the corresponding best fits to residuals with respect to the reference fields of different maximum degrees by choosing appropriate high-frequency attenuation depth parameter D, and low-frequency attenuation depth parameter T. The most important part of the fitting is the part up to the half-power point (or sometimes the zero crossing). What happens to larger lags, as shown by the sinusoidal oscillations in the figure, is less relevant for determination of the covariance function, as the DC effects are primarily affected by the correlation length of the input signal

Once a suitable set of covariance parameters are found, the LSC prediction is carried out to continue the input grids from 6200 m altitude to lower altitudes, at which the predicted values are compared with the corresponding values synthesized from EGM2008. To speed up the computation, OpenMP and fully parallelized matrix inversion and multiplication subroutines are added to the original GRAVSOFT program. Due to RAM limitations, the input grid is 2'x2' that is extracted from 1'x1' data, while the prediction output is a 1'x1' grid to be identical to the outputs from other methods. The 2'x2' spacing is still sufficient for this simulation because the true resolution of simulated input is 5'x5'. The RMS of the differences are shown in Figure 11.

The first thing that needs to be pointed out is that LSC works well for the full field for noise free and noisy datasets. The DC errors for the noisy datasets is less than 1.5 times of the DC errors for the noise free dataset

in contrast to 100 to 1000 times for the ill-posed inverse Poisson results in sub-section 3.2. This is explained by the regularizing effect of the noise covariance matrix (e.g., Rummel et al., 1979). The DC errors are larger for the colored noise dataset for both the full field and the residual field solution (reference field complete to degree 690).

In addition to finding the covariance function parameters, the noise term also determines the quality of the LSC results. Figure 12 shows that the DC error for the noise free input changes with respect to levels of the noise term added to Eq. (A.2.3). For this case, it is known that the data are noise free. However, if $D_{\mathrm{n,n}}$ is set to zero in Eq. (A.2.3), the covariance matrix is getting very close to singular, and the output becomes astronomic numbers and meaningless. Adding appropriate artificial noise helps to stabilize the solution; this highlights the ill-posed problem of the downward continuation process.

4.1.2. SHA

Figure 13 shows the degree variances of the (residual) gravity disturbances after fitting the data over the simulation area into SHA by using the procedures described in Appendix A.1.

We observe that the power of this local field after global zero padding is completely different from the power of the global field. For the full field signal (first row, first column), the peak of the degree variance for the full field data locates around spherical harmonic degree 55, which is about a wavelength of 730 km approximating the dimension of the entire study area. Then the power decreases more or less according to Kaula's rule towards the higher degrees as expected. There are obvious spectral components in the low degrees because of applying the global function for a representation of space-limited data. The noise effects are relatively small. The white noise is more evenly distributed than the colored one in the spectral domain as expected. Due to the strong signal-to-noise ratios, they are not being mistakenly taken into the models so much as to smear the signal. The noisy spectrum becomes more and more significant when removing a higher degree reference field, the signal to noise ratio reduces as there is less signal power in the residual field.

For the residual fields, the corresponding degree variance plots in Figure 13 show the location of the maximum degrees removed. They also show the power due to the GOCO05s updates to EGM2008, especially when a reference field complete to degree 2190 is used.

Figure 14 shows the DC errors for the SHA method. This method models the gravity field with an inherent low-pass filtering process, which effectively stabilizes DCP. It manifests a direct way to compress the large DC errors of high-frequency so that the SHA DC errors are at the comparable magnitude between the noise free and two types of noise input data. The colored noise results show larger errors than the white noise ones because of the differences in their spectral distribution of noise (see Figure 2). Interestingly, this method "works well" even when the "local" coefficients do not match the "global" coefficients. For example, for the case when the reference field is complete to degree 2190, the RMS value of the DC error from 6200 m to the ellipsoid is 0.0189mGal, much smaller than the RMS in the original residuals (σ_(EGM2008-FullxGeoid16refA)=0.298mGal). Because we know the differences between EGM2008 and xGeoid16refA range from degree 2 to 280, the residual coefficients higher than degree 280 reflect spectral representation of SHA for the space-limited data. If the residual coefficients are only used up to degree 280 in the restore step, the RMS mismatch changed from 0.0189 mGal to 0.0431 mGal (red vs red dash lines in the bottom-right graph of Figure 14). Though the RMS values in this case are very small, we know that the "residual coefficients" are not spectrally 'real' in a global sense.

4.3 Case simulation 2: flight lines and surface points

The simulated data in sub-section 3.3.1 are used in this case simulation. Both simulated airborne and surface gravity disturbances have the same spectral content as EGM2008, with the data at the flight level being smoother than the surface data, as a natural consequence of attenuation of gravity field variations with altitude.

Before DC, a reference field was subtracted from the data. The reference field is the XGM18 model complete to spherical harmonic degree 760 (which corresponds to an ellipsoidal harmonic degree of 719) complemented by the Earth2014 model (Rexer et al. 2016) for ellipsoidal harmonic degrees 720 to 2190. The resulting residual field evaluated along the flight trajectories defines the noise-free dataset. Similar to simulation case 1 in sub-subsection 3.2, white and colored noise, respectively, with a standard deviation of 1 mGal were added to the noise free residuals to generate two noisy datasets. All three sets of residual gravity disturbances are downward continued to the surface points of Figure 7. Thereafter, the full downward continued gravity disturbances were computed by restoring the reference field quantities. Gravity disturbances errors were computed as the difference to the ground truth gravity disturbances from EGM2008.

The SHA, inverse Poisson, and ADC methods, use gridded data as input to the downward continuation. First, residual gravity disturbances were generated along the real flight trajectories from EGM2008 - XGM18 - Earth2014. The data were used to compute the parameters of the model covariance function. Using the latter, LSC was used to interpolate the data at the nodes of a 1'x1' grid, which was located at a mean altitude. It should be noted that the inverse Poisson and ADC results are computed in two steps. First, the LSC-predicated airborne grids are downward continued to the surface of the reference ellipsoid. Second, the gravity disturbance residuals are computed by the forward Poisson method at the surface points. The SHA results are computed in a different two-step procedure. First, a spherical harmonic gravitational model is developed, and then the results are synthesized from the model. In contrast, the LSC and RBF results are computed by directly predicting the residuals at the surface points from the flight lines.

The error statistics are shown in Table 1. For noise free data, the error standard deviations range from 0.1 mGal (RBF) to 0.7 mGal (LSC+ADC); using LSC on the full signal gives a worse standard deviation of 1.0 mGal, though the spatial distribution of the errors is heterogeneous which largest errors in mountainous regions where the model covariance differs significantly from the real covariances. The RLSC solution did not perform better than the LSC solution, though the method was developed to improve over LSC (Willberg et al. 2019). For the SHA method, truncating the coefficients below degree 300, where the global model should be dominating the spectrum, will almost double the DC error (0.3 mGal to 0.6 mGal) in the error free case because of the space-limited data.

Table 1. Statistics of DC errors of the six methods at 31,358 surface gravity points (unit: mGal).

Methods	Noise free		1 mGal white noise		1 mGal colored noise	
	mean	std	Mean	std	mean	std
LSC (Full field signal without RCR)	-0.004 (-0.012)	0.320 (0.958)	0.001	1.014	0.086	1.887
LSC+SHA (d/o>300)	0.002 (0.050)	0.346 (0.627)	0.029 (0.033)	1.482 (1.577)	0.087 (0.114)	1.908 (1.998)

LSC+Inverse Poisson	0.007	0.319	0.028	1.463	0.088	1.912
LSC+ADC	0.027	0.689	0.028	1.459	0.072	1.588
RBF	0.000	0.127	0.049	1.307	0.094	1.973
RLSC	-0.015	0.321	0.040	0.934	-0.047	2.133

For white noise data,, LSC and RLSC provide again comparable results (1.0 mGal and 0.9 mGal error standard deviations). The other four methods have error standard deviations which are 30%-50% larger. Unlike simulation case 1, the inverse Poisson and ADC solutions are affected by the white noise only at a moderate level demonstrating that the LSC gridding before downward continuation has a stabilizing effect.

For colored noise data, Moritz's ADC provides the smallest error standard deviations (1.6 mGal); the error standard deviations for the other methods range from 1.9 mGal (LSC, LSC+SHA, LSC+inverse Poisson) to 2.1 mGal (RLSC). The solutions based on colored noise data have significantly larger error standard deviations than the solutions based on white noise data. The LSC DC errors in the three cases are shown here in Figure 15 to illustrate the distribution of DC errors.

A common feature of the DC errors for these methods is the correlation with spatial variation of the gravity field itself. The stronger horizontal gravity gradient the field is, the larger the DC errors. One explanation is that the attenuation of gravity signals at the high flight levels leads to the loss of detail at altitude, which is magnified along with instrumental noise in the DC process. We speculate that less loss may be achieved by the use of RCR scheme with high-quality and extra-high degree EGM models, which regain more details in the restore step. This appears to be the case for the LSC method as shown in Table 1, Figures 15 (top panel) demonstrates for the case of noise free input. It is clear that the LSC method only "breaks down" in several rare spots where the observations have gaps.

5. Results using airborne and surface gravity data

5.1 Gravity validation results

We further evaluate the performance of the various DC methods using the same airborne data set distributed to the Colorado 1 cm geoid experiment project (Wang et al. 2021; Sanchez et al. 2021). Compared to synthetic EGM2008 data, real airborne data are by their nature along-track filtered gravimetry data, which adds additional noise to the comparisons, as does any use of cross-over adjustments of airborne data.

The Colorado GRAV-D airborne data are decimated to every 8 seconds, which result in 35587 airborne data. The same XGM18 reference field and the same topographic effects used in sub-section 4.3 are then removed to generate the gravity disturbance residuals. It is worth noting that the spectral band of the airborne data is limited. If the spectral contents are not matching, all the methods will be subject to the same errors. The NGS shared surface gravity data in the Colorado experiment project are used to validate with the downward continued airborne data. Note that all the duplicated surface points in that study are removed. The XGM18 and topographic effects are also removed so that the residuals are comparable with the downward continued residuals of the GRAV-D data.

To remove the highest frequency information in the surface data that are attenuated in the airborne data, a high-resolution RTM technique (Forsberg 1984) is applied to the surface data. The surface gravity anomalies are converted into gravity disturbances by using EGM2008 geoid values. In general, this evaluation is the same as case simulation 2 in sub-section 4.3 except for that the datasets are real and are identical to those in Willberg (2020).

The DC errors are summarized in Table 2 for all the six methods. Strictly speaking, the GRAV-D data are not directly comparable with the surface gravity data because the former are band-limited due to the high altitude and along-track filtering applied while the latter are surface point observations. In the case of errors negligible in observation and computation, the difference between them largely reflects the omission error of GRAV-D data. Otherwise, the residuals comprise the omission error, observational error, and computational error. Again, only the LSC results are illustrated here in Figure 16. As it can be seen, large errors are mostly associated with higher topography in the region of study where the omission error tends to dominate.

When RTM effects are computed from surface data only, and considering that the spectral band of airborne data does not contain as much high frequency information as the surface data, a high-resolution RTM (Forsberg 1984) effect in the surface data has to be removed to make them spectrally consistent. The question is: "Which degree is considered as the high frequency?". We know the XGM18 and topographic effects below 2190 have been removed. However, we also know that the RTM technique has approximations related to the "harmonic correction" of data points below a smooth mean elevation surface (Forsberg 1984). Thus, we tried several different cut-off degrees to optimize the approximate approach. Figure 17 shows the RTM-corrected RMS differences with respect to the reference spherical harmonic degree for RTM. It is clear that if the reference degree is too low the gravity signal of the topography gets removed twice (once from XGM18 and Earth2014, once from RTM), while if it is set too high some of the high frequency signal is not removed completely. The minimum value is right in the band between degree 2500 and 3000. Though it is not exactly equal to degree 2190, it may be close to this theoretical value. As Figure 17 shows, after applying the RTM correction, RMS of the mismatch is reduced from 11.5 mGal to 5.4 mGal.

Table 2. Statistics of the differences between the downward continued airborne data and surface data without/(with) RTM correction (units: mGal).

methods	Mean	Std.
SHA/(-RTM)	2.7/(-1.0)	11.6/(5.5)
d/o > 300/(-RTM)	2.3/(-1.5)	11.5/(5.6)
LSC(-RTM)	2.7/(-1.0)	11.5/(5.4)
Inverse Poisson 1/(-RTM)	2.7/(-1.0)	11.5/(5.4)
Inverse Poisson 2/(-RTM)	2.7/(-1.1)	11.6/(5.8)
ADC/(-RTM)	2.7/(-1.1)	11.5/(5.5)
RBF/(-RTM)	2.2/(-1.5)	11.4/(5.4)
RLSC/(-RTM)	2.4/(-1.3)	11.9/(5.4)

What we are interested in is the computational error of DC caused by each method. As the residual results from all the methods are subject to the same omission error and observational error, a lower level of residuals indicates a better agreement with the surface gravity data. The residuals shown in Table 2 are similar among all six methods, and the differences are not significant enough to tell which method is the best when taking in consideration the observational errors from the GRAV-D and surface data, which are estimated to be typically 1-2 mGal for each source.

However, LSC has an advantage because it combines regularization and DC into one step through a 3D covariance function and provide comparable results with the other methods. Unlike LSC, RLSC is built upon covariance matrices computed from the reference GGM. RBF is also attractive because it is a local method and can directly operate on scattered data; only in case of larger data gaps, interpolation may be necessary to obtain optimal results. An effective check to the LSC DC is the combination of LSC gridding and Poisson DC to detect systematic biases by LSC alone. Though the Inverse Poisson can start from scattered points too, it has been shown that it is better to start from gridded data (Alberts and Klees, 2004). For the SHA method, truncating the coefficients below degree 300 increases the SHA DC error.

5.2 Geoid results

The geoid models are computed from the gravity disturbances continued onto the reference ellipsoid by (see Appendix B)

$$N(\Omega) = \zeta_0(\Omega) + \zeta_1(\Omega) + \zeta_{\mathrm{Ref}}(\Omega) + d\zeta(\Omega) + C_{\mathrm{T}}(\Omega) \tag{7}$$

where ζ_0 and $\zeta_1$are the degree-0 and degree-1 terms, respectively (Sánchez et al. 2021; Wang et al. 2021); ζ_{Ref} is the height anomaly on the reference ellipsoid (GRS80), which is synthesized from XGM18 and the synthetic topographic geopotential model predicted from Earth2014; and

$$d\zeta(\Omega) = \frac{R}{4\pi\gamma(\Omega)} \int_{\sigma_0} S_{\mathrm{MDB}}(\psi)[\Delta g_{\mathrm{Airborne}}(\Omega') - \Delta g_{\mathrm{Ref}}(\Omega')]d\sigma \tag{8}$$

where $\gamma(\Omega)$ is the normal gravity on the reference ellipsoid; S_{MDB} a modified degree-banded Stokes kernel function which spans from spherical harmonic degree 210 to 2160 with transitional bands of 60 and 120 degrees at the low and high ends, respectively (Huang, and Véronneau 2013). Δg_{Ref} is the gravity anomaly on the reference ellipsoid synthesized from XGM18 and the synthetic topographic geopotential model predicted from Earth2014 too. The full airborne gravity disturbance continued onto the reference ellipsoid is transformed into the gravity anomaly by

$$\Delta g_{\mathrm{Airborne}}(\Omega) = \delta g_{\mathrm{Airborne}}(\Omega) - 0.3086 N_{\mathrm{CGG2013}}(\Omega) \tag{40}$$

The term C_{T} transforms the height anomaly evaluated on the reference ellipsoid into the geoid height.

The resulting geoid models are validated using the GSVS17 GPS-levelling data in the region of study (van Westrum et al. 2021). The results are shown in Figure 18. As it can be seen that all the methods have a similar performance except for two cases. The case of Poisson1 gives a slightly poor agreement, in which the DC threshold value is set as 1 mGal to reflect the data error. The other case is for SHA300, in which the spherical harmonic model is truncated to degree 300. These geoid validation results are consistent with the gravity ones in sub-section 5.1.

6. Summary and conclusions

Downward continuing airborne gravity data from flight heights onto the surface of the Earth or a level surface, from scattered points into regular sampled grids, enables the direct use of the classical geoid procedures that is based on Stokes's integrals. However, this downward continuation procedure is not a trivial task due to the instability of this procedure. Four classical DC methods and two relatively newer approaches have been tested using both simulated data and real data.

For the simulation tests, both regular sampled grids and scattered points are used in two cases of noise scenarios. If the data are regularly sampled and noise free, all methods perform reasonably well, except for an artificial noise term which needs to be added to LSC to avoid round-off error amplification. These ideal

data sets are used to verify the correctness of the developed software that can be shared on request. For the SHA approach, all of the spectrum of the real gravity field is distorted. The reason is that when fitting a SH model to a space-limited dataset, the power in the signal is distributed over all frequency (i.e., over the SH coefficients) providing a power spectrum which differs completely from the power spectrum of the global dataset. The least-squares constraint does not control the spectrum when minimizing the residuals. This casts a heavy doubt on any method that tries to directly combine a global gravity field and local gravity field in the spherical harmonic domain.

In the white noise and colored noise cases, the performances of all methods are degraded; the inverse Poisson becomes unstable, while Moritz's ADC diverges. However, the covariance matrix in LSC and the linear solver in SHA can still control the noise effects to reasonable magnitudes. For the LSC, an accurate estimation of the noise level is equally important as the estimation of the covariance functions. The tests on the gridded data prove that there are no major problems in the developed software, i.e., no bugs in the codes.

For the simulated tests on scattered points, the RBF gives the best results in the error free case. Even in the white and colored noise cases, RBF still performs reasonably well if the data is band-limited. Further improvements are expected when using a more careful RBF network design and a regularized weighted least-squares estimator instead of the un-regularized ordinary least squares estimator (e.g., Slobbe 2013, Slobbe et al 2019).

In the real data tests, the residual gravity disturbances are not band-limited in the spectral range after removing the GGM and Earth2014. This is a typical situation in airborne data applications, where the goal exactly is to detect problems in medium-wavelength gravity field variations. In the Colorado case, the different methods gave similar results, mainly due to the unavoidable errors in airborne data, and the relatively high flight level.

We note that due to the lack of band-limited data, the current implementation of RBF cannot efficiently distinguish signal from noise, which is also true for inverse Poisson. The afore-mentioned improvements may provide a significantly better RBF solution. We also note that both the simulated tests and the real tests do not show significant numerical improvement from LSC to RLSC, though the latter has some theoretical advantages, but also requires more intense computational effort to establish the complicated covariance matrices. This casts a doubt on the practical application of this improved LSC method for airborne gravity data.

The geoid models are computed from the DC results from all the methods, and are validated by the GSVS GPS-levelling data. They show a similar agreement around 3 cm r.m.s., with LSC performing marginally better than the other methods. Giving the rough topography in the Colorado areas this is a good result, but also highlight the limits of high-level airborne gravity data in terms on reaching a 1 cm-geoid as a stand-alone data source without supplementary surface gravimetry data.

Author Contribution Conception or design of the work was contributed by XL, JH, RK, RF, MW, CS, RP, and CH; Data analysis was done by XL; Geoid modeling was done by JH; Writing—orginal draft preparation was contributed by XL and JH; Writing—review and editing were done by RF, RF, MW, and CH; Critical revisions of the article were done by RK and JH.

References cited in the main text

Alberts B, Klees R (2004) A comparison of methods for the inversion of airborne gravity data. Journal of Geodesy 78, 55–65.

Cai J, Grafarend EW, Schaffrin B (2004) The A-optimal regularization parameter in uniform Tykhonov-Phillips regularization — α-weighted BLE-. In: Sansò F. (eds) V Hotine-Marussi Symposium on Mathematical Geodesy. International Association of Geodesy Symposia, vol 127. Springer, Berlin, Heidelberg. https://doi.org/10.1007/978-3-662-10735-5_41

Darbeheshti N, Featherstone WE (2010) A review of non-stationary spatial methods for geodetic least-squares collocation. J Spat Sci 55(2):185–204.

Forsberg R (1987) A new covariance model for inertial gravimetry and gradiometry, J. Geophys. Res., 92(B2), 1305–1310.

GRAV-D Team (2017a). "GRAV-D General Airborne Gravity Data User Manual." Theresa Damiani, Monica Youngman, and Jeffery Johnson ed. Version 2.1. Available DATE. Online at: http://www.ngs.noaa.gov/GRAV-D/data_MS05.shtml

GRAV-D Team (2017b). "Block MS05 (Mountain South 05); GRAV-D Airborne Gravity Data User Manual." Monica A. Youngman and Jeffery A Johnson. BETA Available DATE. Online at: http://www.ngs.noaa.gov/GRAV-D/data_MS05.shtml

Heiskanen WA, Moritz H (1967) Physical geodesy. Bull. Geodesique 86, 491–492 .

Holmes SA (2016) Using Spherical Harmonic Expansions for Geopotential Modeling with Airborne Gravity, 2016 Airborne Gravimetry for Geodesy Summer School, May 23-27, 2016, in Silver Spring, Maryland, https://www.ngs.noaa.gov/GRAV-D/2016SummerSchool/

Jiang T, Li J, Wang Z et al (2011) Solution of ill-posed Problem in Downward Continuation of Airborne Data, Acta Geodaetica et Cartographica Sinica, 40(6) 684-689.

Jekeli C (1981) The downward continuation to the Earth's surface of truncated spherical and sllipsoidal harmonic series of the gravity and height anomalies, OSU Rep. 323, Dept. of Geodetic Science and Surveying, The Ohio State Univ., Columbus

Jekeli C (1981) Alternative methods to smooth the Earth's gravity field, OSU Rep. 327, Dept. of Geodetic Science and Surveying, The Ohio State Univ., Columbus

Jekeli C (2010) Correlation Modeling of the Gravity Field in Classical Geodesy. In: Freeden W., Nashed M.Z., Sonar T. (eds) Handbook of Geomathematics. Springer, Berlin, Heidelberg. https://doi.org/10.1007/978-3-642-01546-5_28.

Kaula WM (1959) Statistical and Harmonic Analysis of Gravity. J. Geoph. Res., 64, 2401.

Kern, M. (2003). An analysis of the combination and downward continuation of satellite, airborne and terrestrial gravity data. University of Calgary, Calgary, AB. doi:10.11575/PRISM/22980

Klees R, Tenzer R, Prutkin I, Wittwer T (2008) A data-driven approach to local gravity field modeling using spherical radial basis functions. J Geod 82:457–471.

Krarup T(1969) A contribution to the mathematical foundation of physical geodesy. Geodetisk Institut, Copenhagen.

Kusche J, Klees R (2002) Regularization of gravity field estimation from satellite gravity gradients. Journal of Geodesy 76:359–368.

Li X (2018) Using radial basis functions in airborne gravimetry for local geoid improvement. J Geod 92, 471–485.

Lieb V, Schmidt M, Dettmering D, Börger K (2016) Combination of various observation techniques for regional modeling of the gravity field. J Geophys Res 121(5):3825–3845.

Liu M, Huang M, Ouyang Y et al (2016) Test and Analysis of Downward Continuation Models for Airborne Gravity Data with Regard to the Effect of Topographic Height [J] . Acta Geodaetica et Cartographica Sinica, 45(5) 521-530.

Liu Q, Schmidt M, Sánchez L et al., (2020). Regional gravity field refinement for (quasi-) geoid determination based on spherical radial basis functions in Colorado. J Geod 94, 99.

Martinec Z (1996) Stability investigations of a discrete downward continuation problem for geoid determination in the Canadian Rocky Mountains. Journal of Geodesy 70, 805–828.

Milbert DG (1999) The dilemma of downward continuation. AGU 1999spring meeting, 1–4 June, 1999, Boston.

Moritz H (1972) Advanced Least-Squares Methods, Dep. of Geodetic Science and Surveying, Ohio State Univ. Rep. No. 175.

Moritz H (1980) Advanced Physical Geodesy. Karlsruhe: Wichmann Verlag, 499p.

Novák P, Heck B (2002) Downward continuation and geoid determination based on band-limited airborne gravity data. J Geod,76: 269–278.

Novák P., Kern M., Schwarz K.P., Sideris M.G., Heck B., Ferguson S., Hammada Y. and Wei M.,

2003. On geoid determination from airborne gravity. J. Geodesy, 76, 510-522

Pavlis NK, Holmes SA, Kenyon SC, Factor JK (2012) The development and evaluation of the Earth Gravitational Model 2008 (EGM2008), J. Geophys. Res., 117, B04406, doi:10.1029/ 2011JB008916.

Rexer M, Hirt C, Claessens S, Tenzer R (2016) Layer-Based Modelling of the Earth's Gravitational Potential up to 10-km Scale in Spherical Harmonics in Spherical and Ellipsoidal Approximation. Surv Geophys, 37(6): 1035-1074. doi 10.1007/s10712-016-9382-2.

Rummel R, Schwarz KP, Gerstl M (1979) Least square collocation and regularization, Belletin Geodesique, 53, 343-361.

Schmidt M, Fengler M, Mayer-Guerr T, Eicker A, Kusche J, Sanchez L, Han SC (2007) Regional gravity field modeling in terms of spherical base functions. J Geod 81(1):17–38. doi:10.1007/s00190-006-0101-5.

Schwarz KP (1978) Geodetic improperly posed problems and their regularization, Lecture Notes of the Second Int. School of Advance Geodesy, Erice.

Slobbe DC (2013) Roadmap to a mutually consistent set of offshore vertical reference frames. PhD thesis, Delft University of Technology.

Slobbe DC, Klees R, Farahani HH, Huisman L, Alberts B, Voet P, de Doncker F (2019) The impact of noise in a GRACE/GOCE global gravity model on a local quasi-geoid. JGR Solid Earth, 124 (3), 3219-3237, doi 10.1029/2018JB016470.

Smith DA, Holmes SA, Li X, et al. (2013) Confirming regional 1 cm differential geoid accuracy from airborne gravimetry: the Geoid Slope Validation Survey of 2011. J Geod 87, 885–907.

Tscherning CC, Rapp RH (1974) Closed Covariance Expressions for Gravity Anomalies, Geoid Undulations, and Deflections of the Vertical Implied by Anomaly Degree Variance Models. Dep. of Geodetic Science and Surveying, Ohio State Univ. Rep. No. 208.

Tscherning CC (2013) Geoid Determination by 3D Least-Squares Collocation. In: Sansò F., Sideris M. (eds) Geoid Determination. Lecture Notes in Earth System Sciences, vol 110. Springer, Berlin, Heidelberg.

van Westrum D, Ahlgren K, Hirt C and Guillaume S (2021) A Geoid Slope Validation Survey (2017) in the rugged terrain of Colorado, USA. J Geod 95, 9, https://doi.org/10.1007/s00190-020-01463-8.

Vaníček P, Sun W, Ong P (1996) Downward continuation of Helmert's gravity. Journal of Geodesy 71, 21–34.

Willberg M, Zingerle P, Pail R (2019) Residual least-squares collocation: use of covariance matrices from high-resolution global geopotential models. J Geod 93, 1739–1757.

Willberg, M., Zingerle, P. & Pail, R. Integration of airborne gravimetry data filtering into residual least-squares collocation: example from the 1 cm geoid experiment. J Geod 94, 75 (2020).

Xu P, Rummel R (1994) Generalized ridge regression with applications in determination of potential fields. Manuscripta Geodaetica 20:8–20.

References cited in the appendices or supplemental information

Brockwell JP, Davis RA (1991) Time Series: Theory and Methods, New York: Springer Verlag.

Eicker, J. Schall, J. Kusche (2013) Regional gravity modelling from spaceborne data: case studies with GOCE, Geophysical Journal International, Volume 196, Issue 3, Pages 1431–1440, https://doi.org/10.1093/gji/ggt485

Foroughi I, Abdolreza S, Novák P, Santos MC (2018) "Application of Radial Basis Functions for Height Datum Unification" Geosciences 8, no. 10: 369.

Forsberg R (1984) A study of terrain reductions, density anomalies and geophysical inversion methods in gravity field modelling, Dept. of Geod. Sci. Rep., Rep. 355, Ohio State University.

Forsberg R (1986) Spectral Properties of the Gravity Field in the Nordic Countries. Boll. Geodesia e Sc. Aff., Vol. XLV, pp. 361 384.

Forsberg R, Kaminskis J, Solheim D(1996) Geoid of the Nordic and Baltic Region from Gravimetry and Satellite Altimetry, in Gravity Geoid and Marine Geodesy, edited by J. Segawa, H. Fujimoto, and S. Okubo, IAG Symposium Series 117, pp. 540–547, Springer Verlag.

Forsberg R, Olesen A, Keller K (1999) Airborne Gravity Survey of the North Greenland Shelf 1998, Technical Report no. 10, 34 pp., Kort og Matrikelstyrelsen, Copenhagen.

Forsberg R, Olesen A, Bastos L, et al. (2000) Airborne geoid determination. Earth Planet Sp 52, 863–866.

Forsberg R (2002) Downward continuation of airborne gravity data. The 3rd meeting of the International Gravity and Geoid Commission 'Gravity and Geoid 2002', Thessaloniki, Greece.

Forsberg R (2003) Downward continuation of airborne gravity data. Gravity and Geoid 2002, 3rd Meeting of the International Gravity and Geoid Commission (IGGC), Tziavos (ed.), pp51-56, Thessaloniki, Greece August 26-30, 2002, ZITI EDITIONS, THESSALONIKI, GREECE, ISBN: 960-431-852-7.

Forsberg, R., and C. C. Tscherning (2014) An overview manual of the GRAVSOFT geodetic gravity field modelling programs, https://ftp.space.dtu.dk/pub/RF/gravsoft_manual2014.pdf.

Jekeli C (1988) The exact transformation between ellipsoidal and spherical harmonic expansions, Manuscr. Geod., 13, 106–113.

Haagmans RHN, van Gelderen M (1991) Error variances–covariances of GEM-TI: their characteristics and implications in geoid computation.´J Geophys Res 96(B12):20011–20022.

Hofmann-Wellenhof B, Moritz H (2005) Physical Geodesy, Springer-Verlag Wien.

Huang J, Véronneau M, Crowley JW (2019) Experimental Determination of Geoid Models and Geopotentials in the US Rocky Mountains and Interior Plains: Canadian Geodetic Survey's Results, 27th IUGG General Assembly, July 8-18, 2019, Montréal, Québec, Canada.

Huang J, Véronneau M (2015) Assessments of Recent GRACE and GOCE Release 5 Global Geopotential Models in Canada. Newton's Bulletin, N. 5, 127-148.

Huang J, Véronneau M (2013) Canadian gravimetric geoid model 2010. J. Geod., 87:771–790, doi:10.1007/s00190-013-0645-0.

Huang J, Véronneau M (2005) Applications of downward-continuation in gravimetric geoid modeling: case studies in Western Canada. J Geodesy 79, 135–145.

Huang J (2002) Computational Methods for the Discrete Downward Continuation of the Earth Gravity and Effects of Lateral Topographical Mass Density Variation on Gravity and Geoid. PhD Thesis, Department of Geodesy and Geomatics Engineering, The University of New Brunswick, Fredericton, Canada.

Hwang C, Hsiao YS, Shih HC, Yang M, Chen KH, Forsberg R, Olesen AV (2007) Geodetic and geophysical results from a Taiwan airborne gravity survey: Data reduction and accuracy assessment, J. Geophys. Res., 112, B04407, doi:10.1029/2005JB004220.

Kingdon R, Vaníček P (2011) Poisson downward continuation solution by the Jacobi method. J. Geodet. Sci., 1, 74-81, DOI: 10.2478/v10156-010-0009-0.

Klees R, Slobbe DC, Farahani HH (2018) A methodology for least-squares local quasi-geoid modelling using a noisy satellite-only gravity field model. J Geod 92, 431–442 . https://doi.org/10.1007/s00190-017-1076-0

Klees R, Slobbe DC, Farahani HH (2019) How to deal with the high condition number of the noise covariance matrix of gravity field functionals synthesised from a satellite-only global gravity field model?. J Geod 93, 29–44. https://doi.org/10.1007/s00190-018-1136-0

Li X (2009) Comparing the Kalman filter with a Monte Carlo-based artificial neural network in the INS/GPS vector gravimetric system. J Geod 83, 797–804.

Li X (2011) Strapdown INS/DGPS airborne gravimetry tests in the Gulf of Mexico. J Geod 85, 597-605.

Li X, Crowley JW, Holmes SA, Wang YM (2016) The contribution of the GRAV-D airborne gravity to geoid determination in the Great Lakes region. Geophys Res Lett 43:4358–4365.

Lin M, Denker H, Müller J (2019) A comparison of fixed- and free-positioned point mass methods for regional gravity field modeling, Journal of Geodynamics,Volume 125,Pages 32-47,ISSN 0264-3707, https://doi.org/10.1016/j.jog.2019.01.001.

Liu X, Zhongmiao S, Xu K, Ouyang M (2017) Downward continuation of airborne gravimetry data based on Poisson integral iteration method, doi 10.1016/j.geog.2017.03.009

Martinec Z (1996) Stability investigations of a discrete downward continuation problem for geoid determination in the Canadian Rocky Mountains. Journal of Geodesy 70, 805–828.

Naeimi M (2013) Inversion of satellite gravity data using spherical radial base functions, PhD thesis, Munchen.

Pail R, Reguzzoni M, Sansò F,KühtreiberN(2010) On the combination of global and local data in collocation theory. Stud Geophys Geod 54(2):195–218.

Pavlis NK (1998) The block-diagonal least-squares approach, in Development and preliminary investigation, in The Development of the Joint NASA GSFC and the National Imagery and Mapping. Agency (NIMA) Geopotential Model EGM96, NASA Tech. Publ., TP-1998-206861, sect. 8.2.2, pp. 8-4–8-5, NASA Goddard Space Flight Cent., Washington, D. C.

Sánchez L, Ågren J, Huang, J. et al. (2021) Strategy for the realisation of the International Height Reference System (IHRS). J Geod 95, 33. https://doi.org/10.1007/s00190-021-01481-0

Schaffrin B (2006) A note on constrained total least-squares estimation. Linear Algebra Appl 417(1): 245–258.

Sjöberg LE (2007) The topographic bias by analytical continuation in physical geodesy. J. Geod. 81:345–350, doi:10.1007/s00190-006-0112-2.

Wu Y, Abulaitijiang A, Featherstone WE (2019) Coastal gravity field refinement by combining airborne and ground-based data. J Geod 93, 2569–2584.

Zhao Q, Xu X, Forsberg R, Strykowski G (2018) Improvement of downward continuation values of airborne gravity data in Taiwan, Remote Sensing, 10, 1951

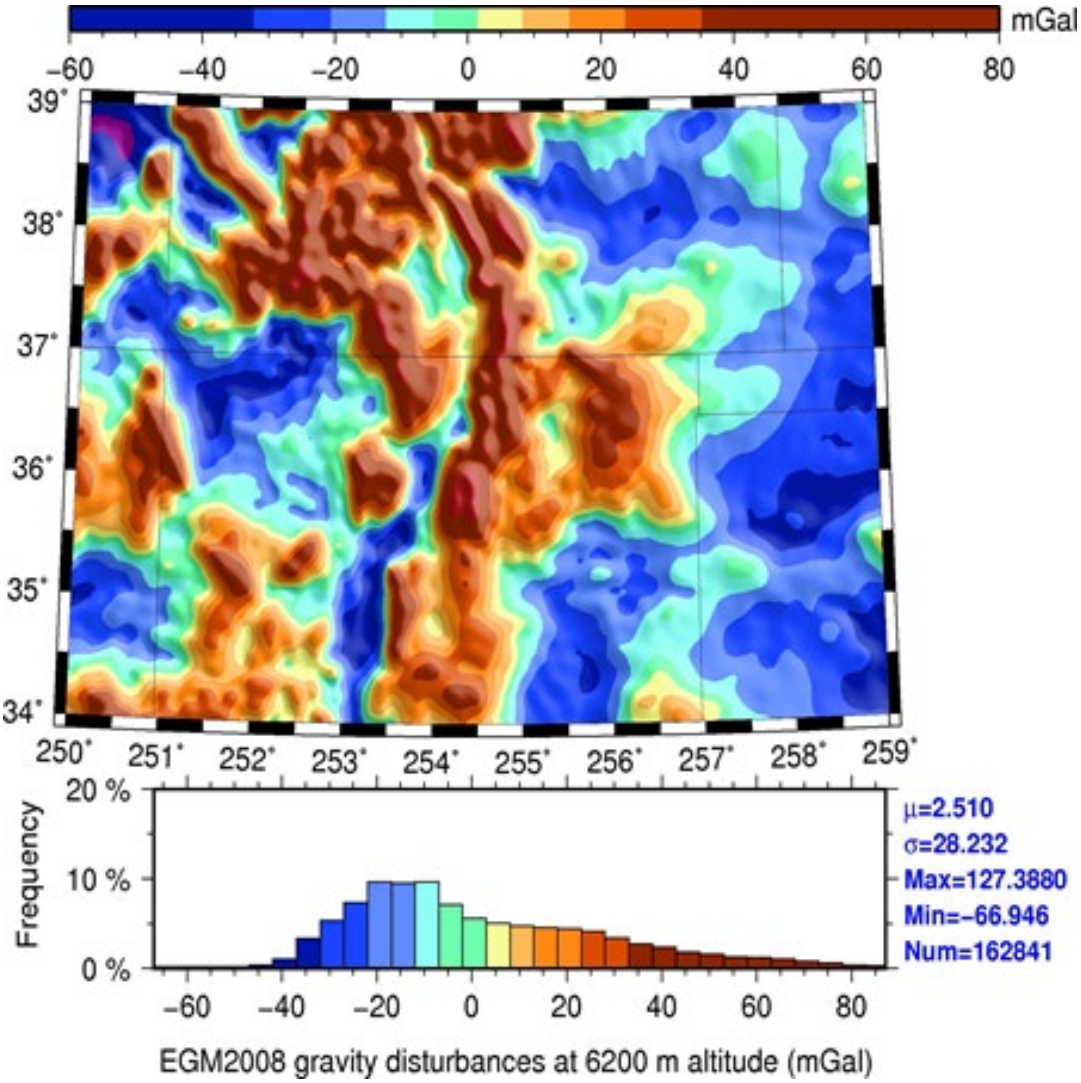

Figure 1. Simulated gravity disturbances from EGM2008 at an altitude of 6200 m.

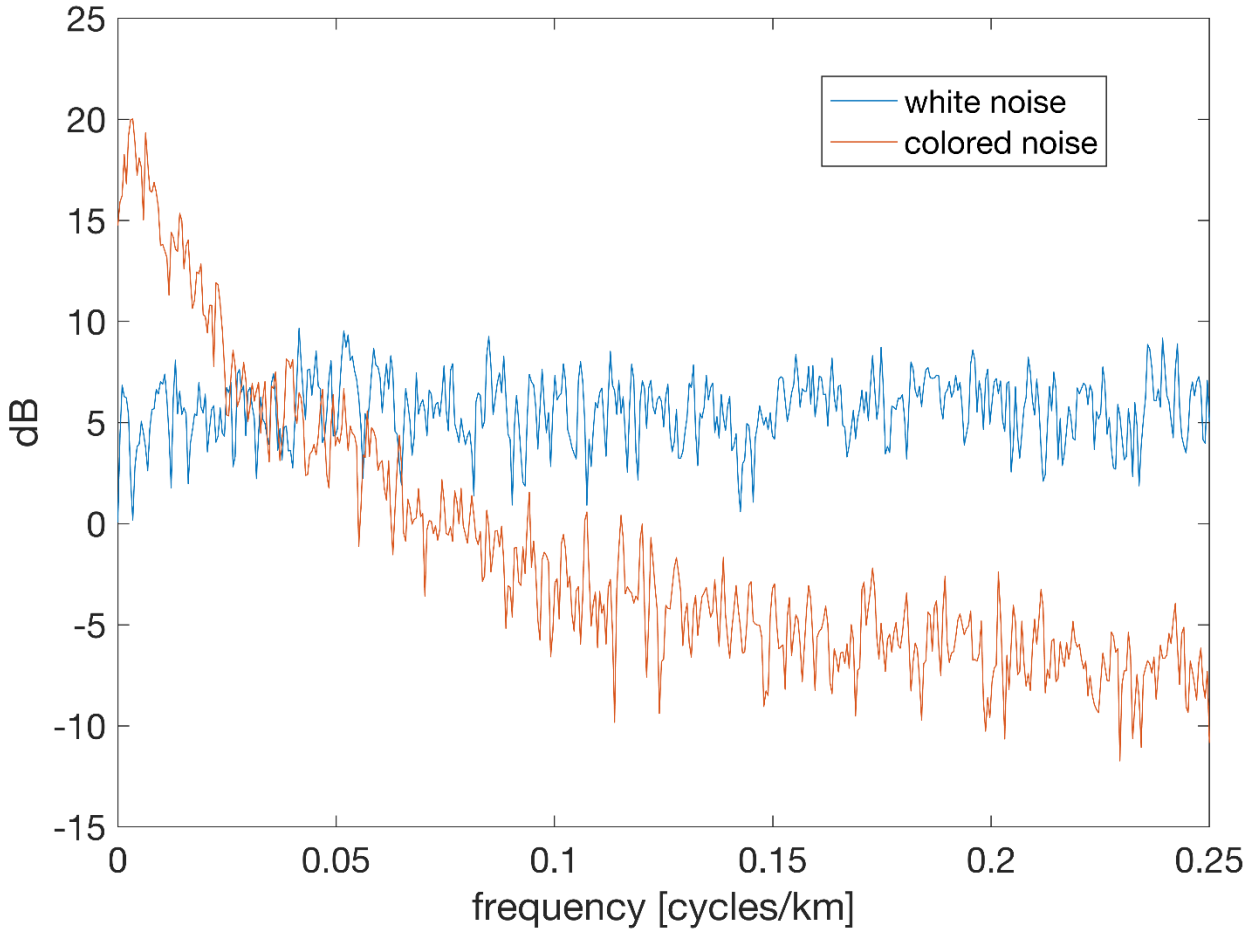

Figure 2. One-Sided Welch periodogram of (bandlimited) white noise and colored noise realizations, respectively. The noise standard deviation is 1 mGal in both cases. The noise realizations were used to generate two noisy gravity datasets.

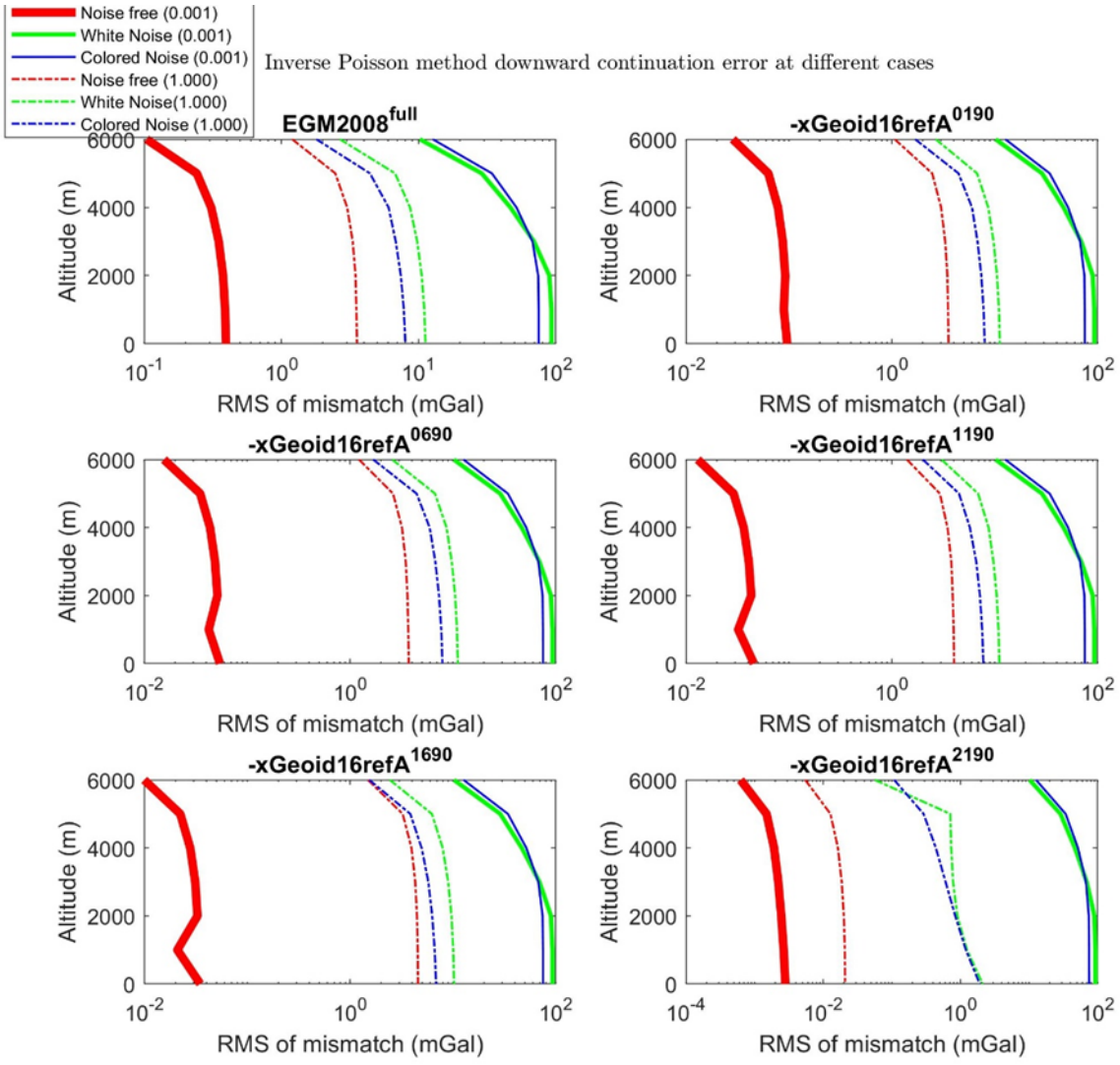

Figure 3. The Poisson DC errors as function of altitude for different reference fields removed and the two types of noise added to the data.

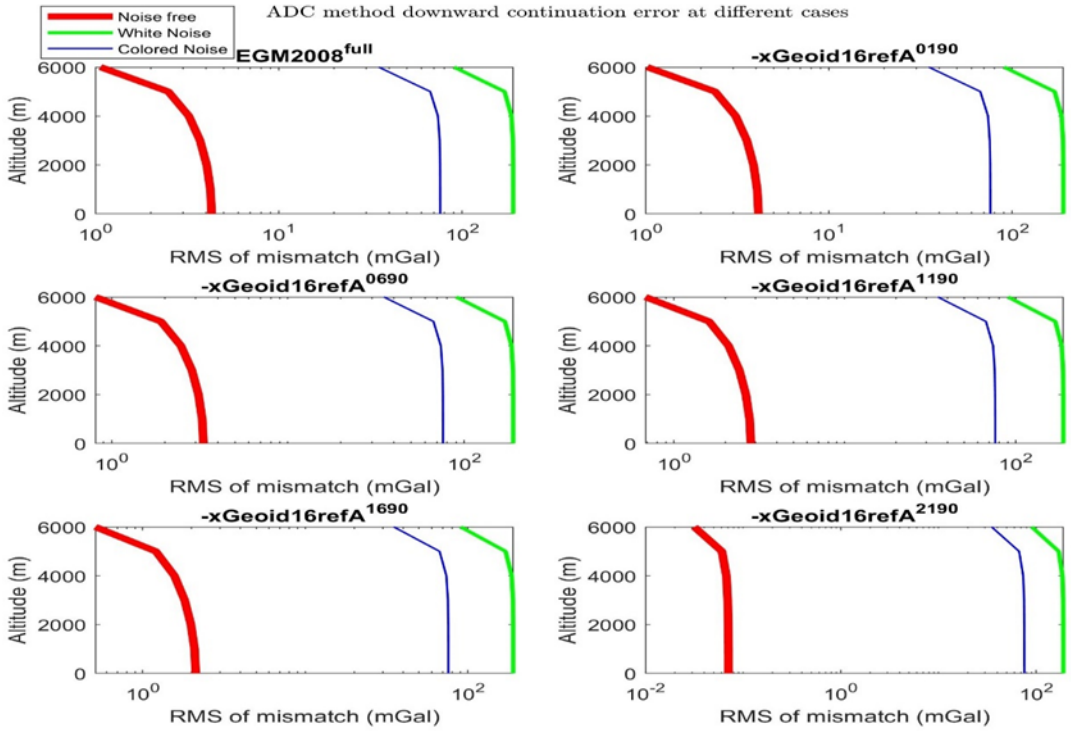

Figure 4. Moritz's ADC DC errors as function of the altitude for different degree and order of reference fields removed and the two types of added noise.

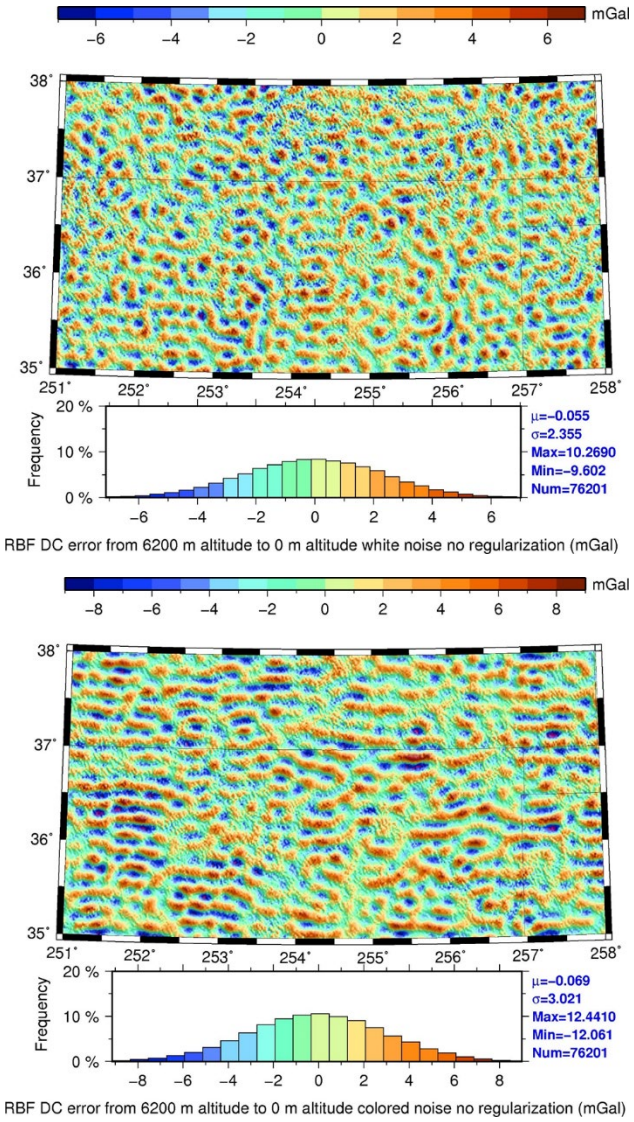

Figure 5. RBF DC errors for adding white noise (top) and colored noise (bottom) to the simulated input gravity data at an altitude of 6200 m.

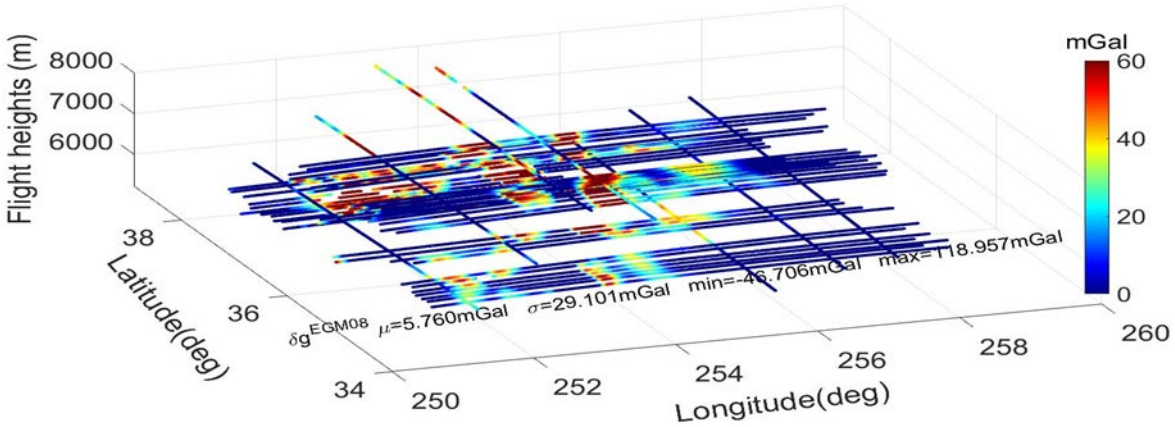

Figure 6. Simulated EGM2008 gravity disturbances along real flight trajectories.

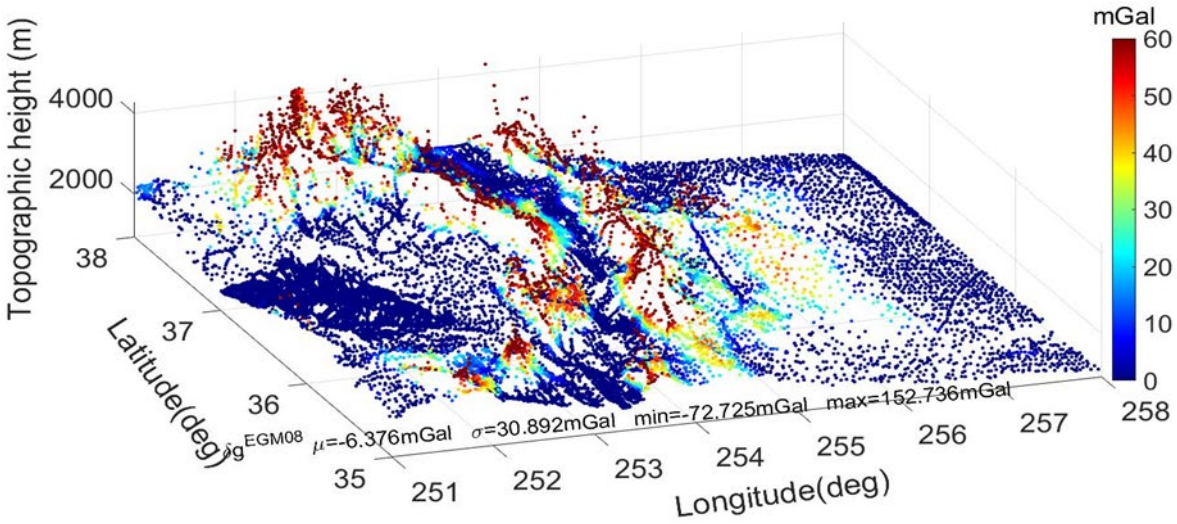

Figure 7. The simulated gravity disturbances at 31,358 points on the topography as ground truth.

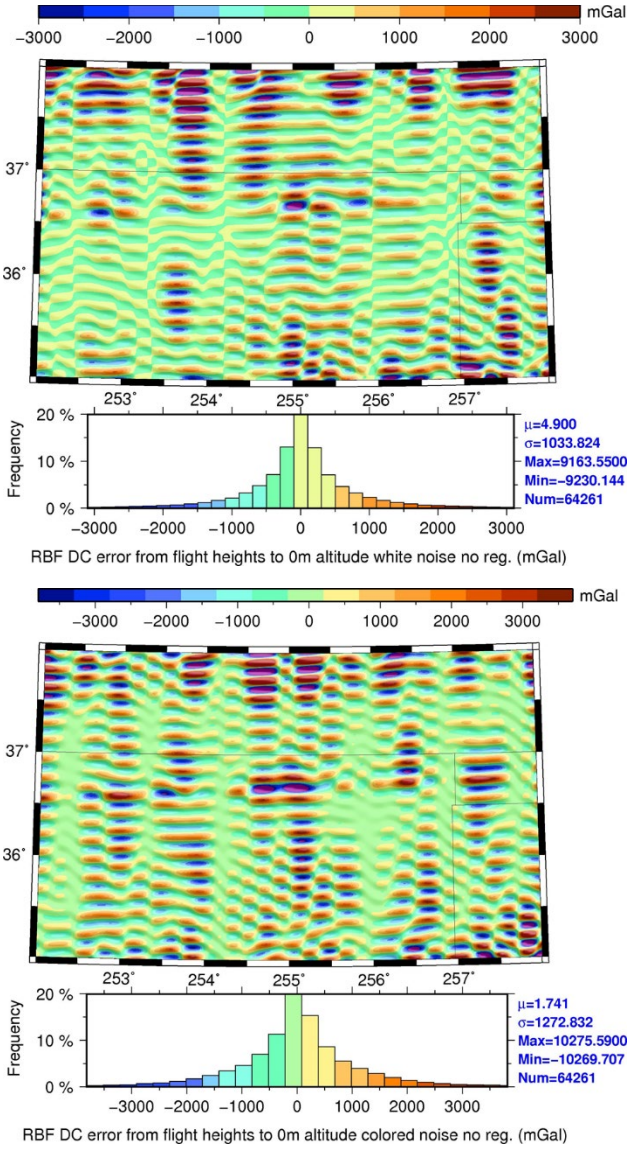

Figure 8. RBF DC errors on the reference ellipsoid for adding white noise (top) and colored noise (bottom) to the simulated input gravity data at the flight lines.

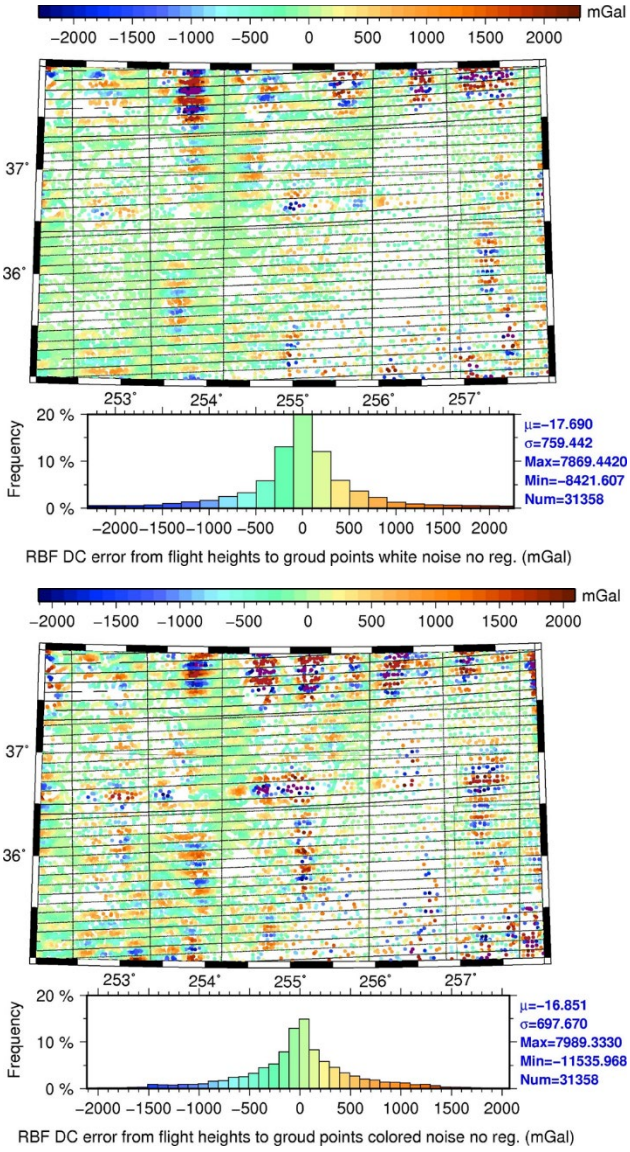

Figure 9. RBF DC errors at the surface points for adding white noise (top) and colored noise (bottom) to the simulated input gravity data at the flight lines.

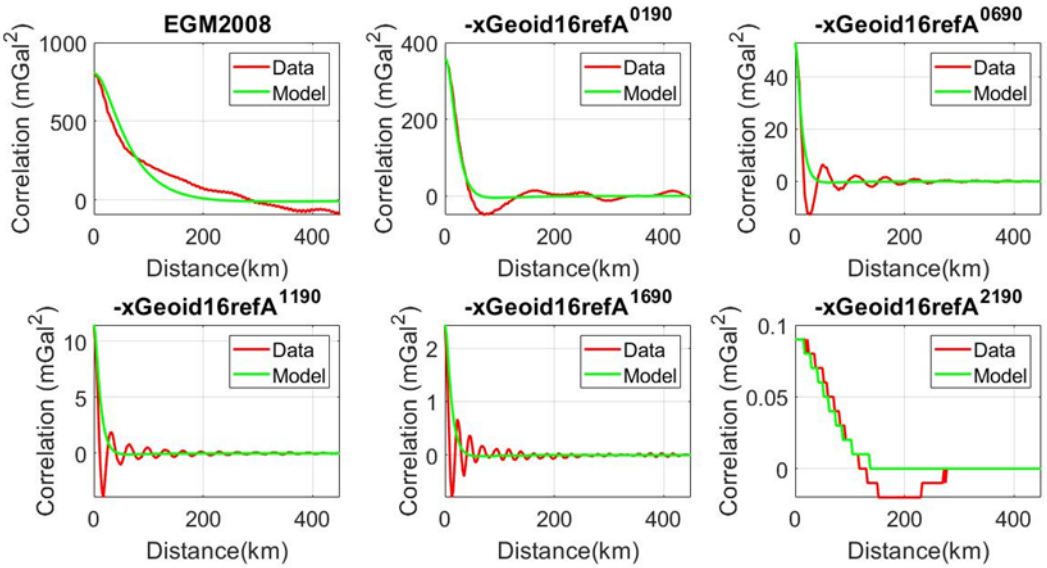

Figure 10. The empirical covariance functions and fitted model covariances fordifference scenarios.

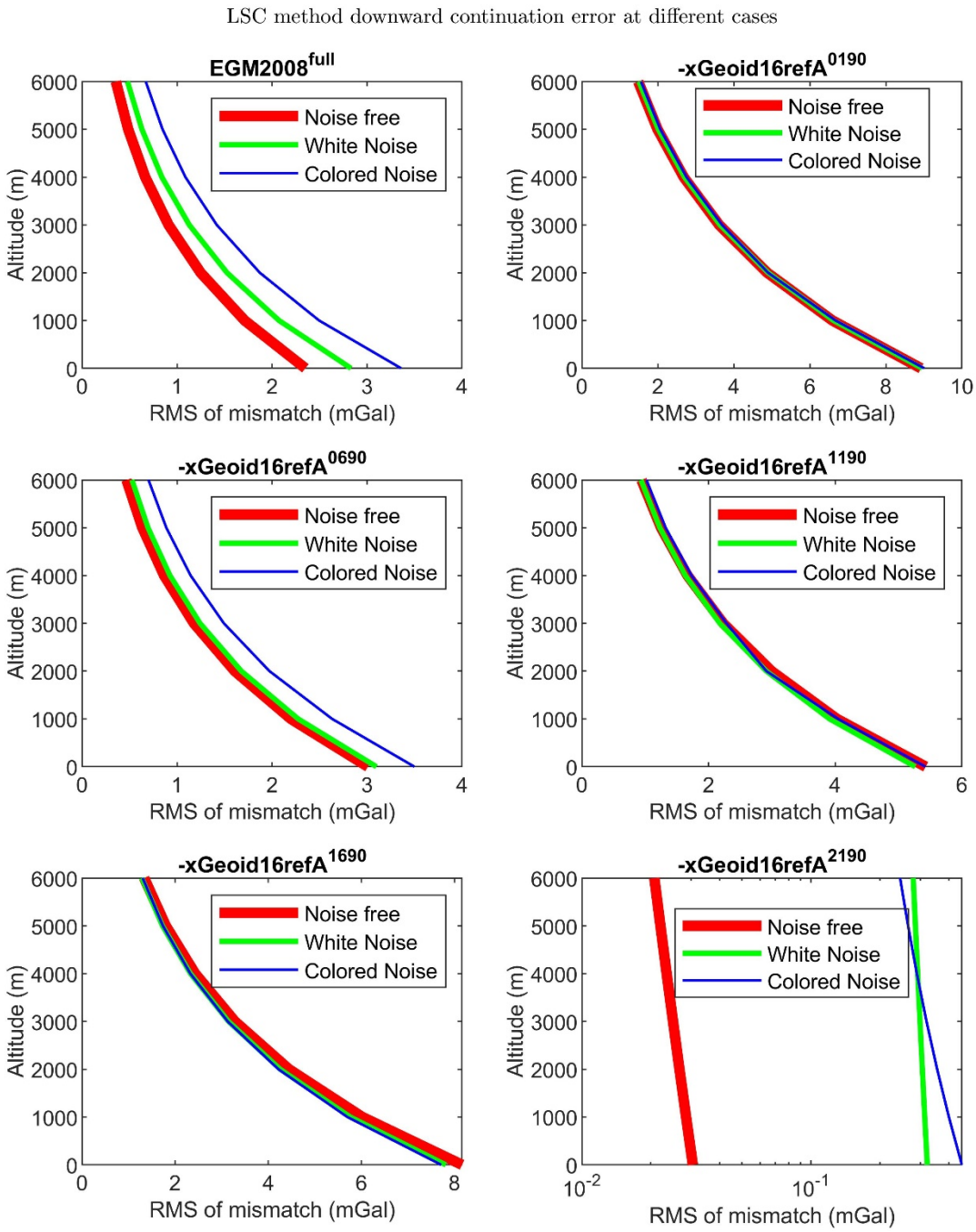

Figure 11. LSC DC errors as function of altitude for the reference fields of different maximum degrees and the two types of data noise.

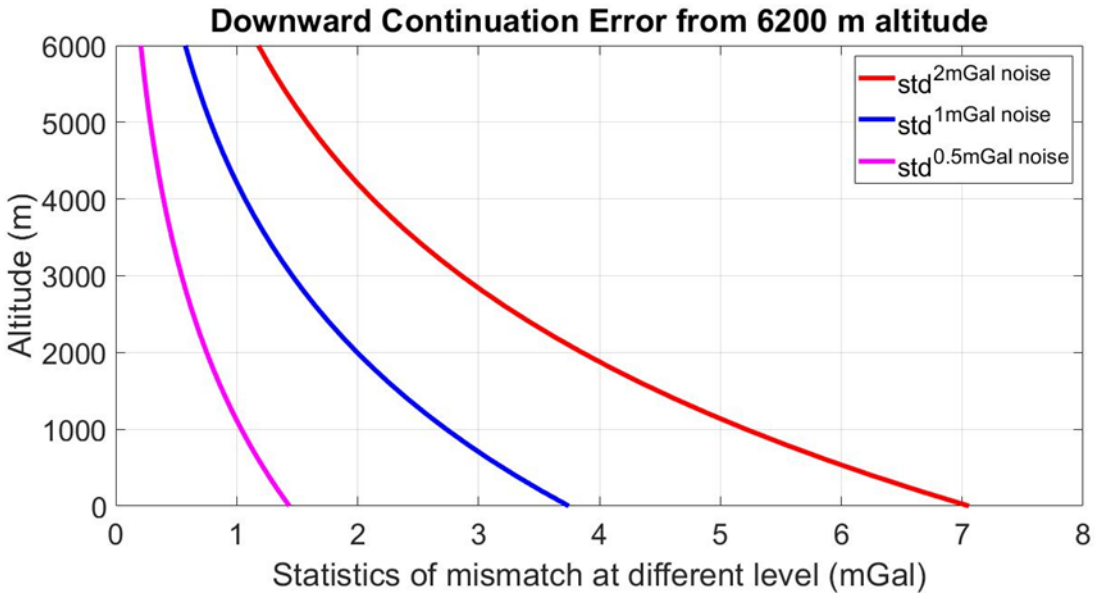

Figure 12. Effect of the choice of the Dn parameter on LSC downward continuation for the noise free input as function of altitude (DC errors with Dn values of 0.5, 1, and 2mGal are represented by purple, blue and red thick lines, respectively).

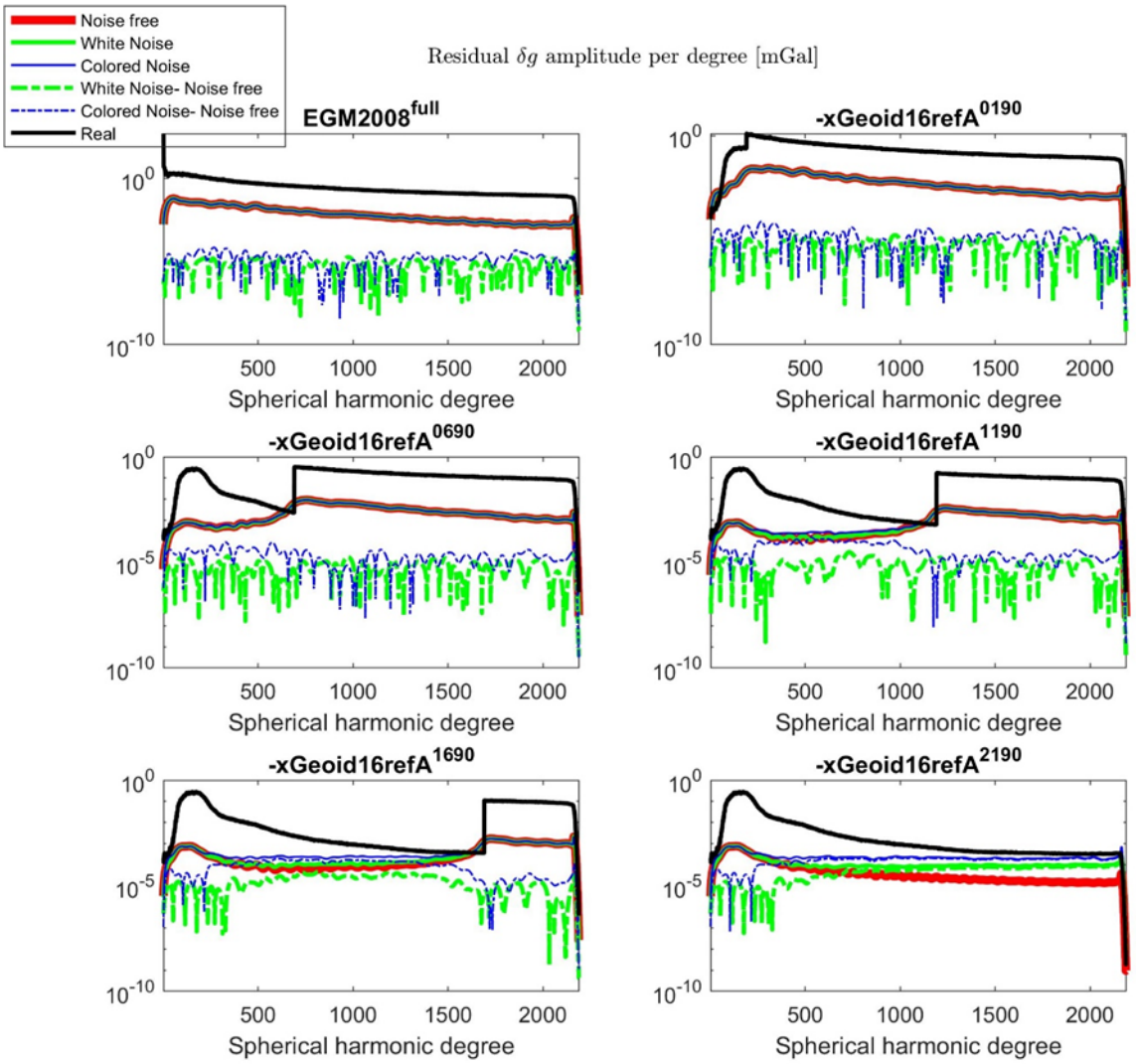

Figure 13. Degree variances of the SHA models from the simulated input data after removing xGeoid16refA truncated at various spherical harmonic degrees.

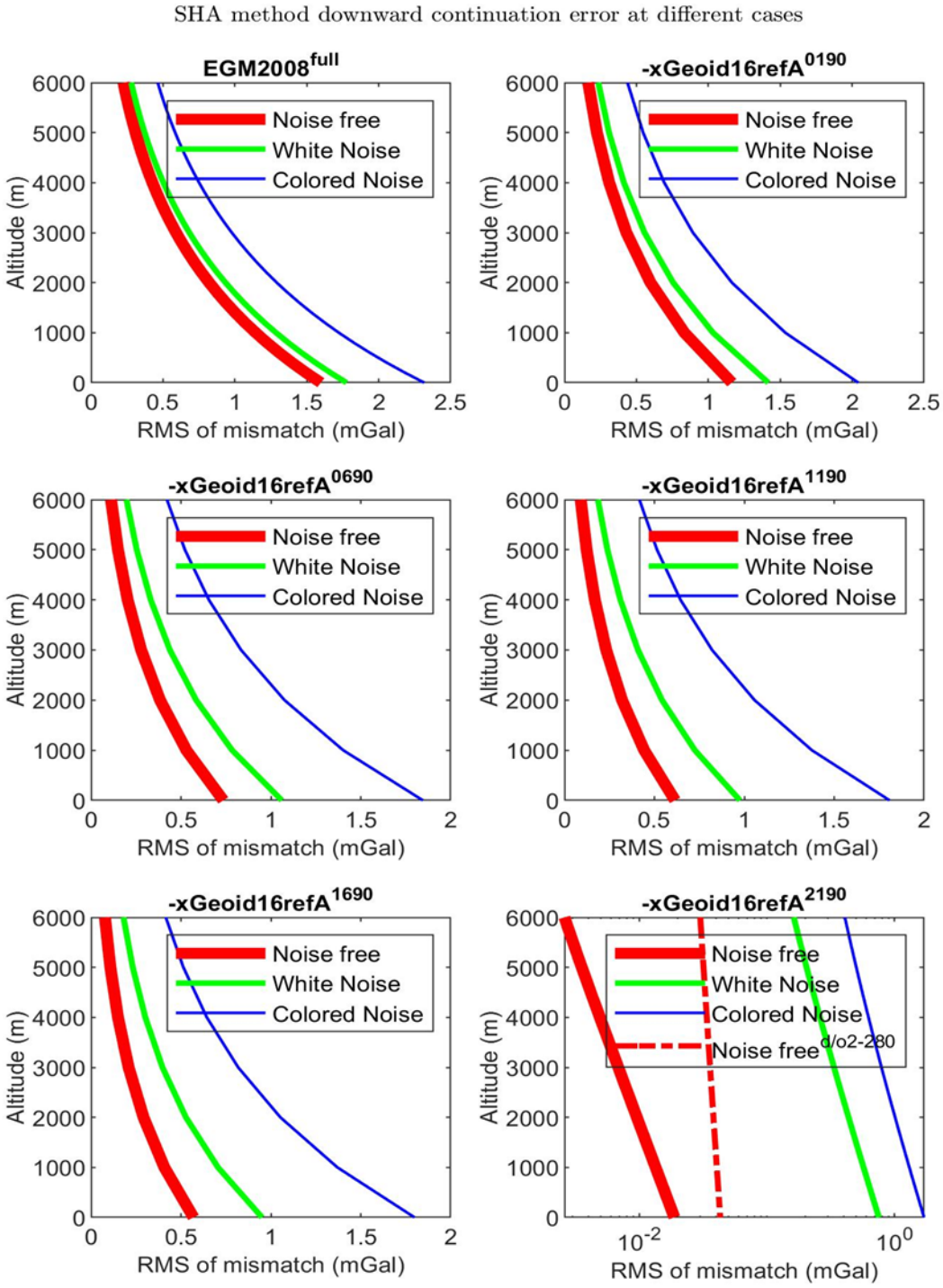

Figure 14. The SHA DC errors as function of altitude for the reference fields of different degrees and the two types of data noise.

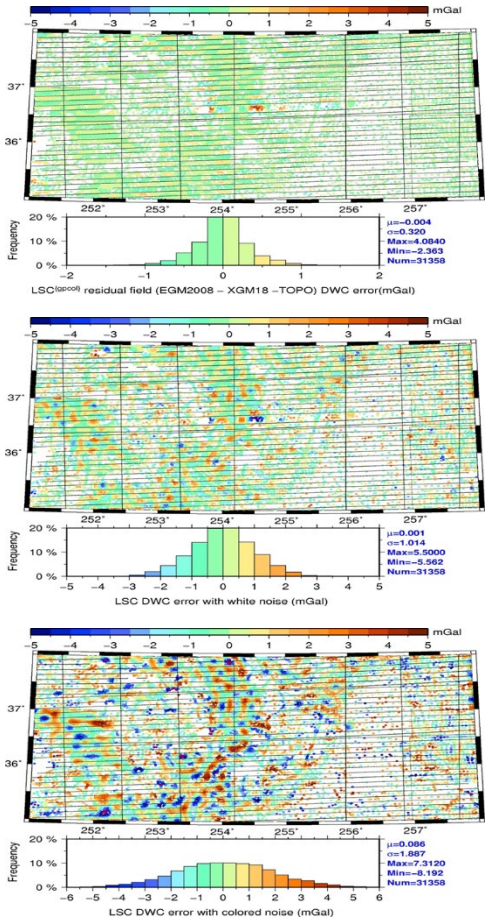

Figure 15. DC errors of LSC for three datasets: noise free (top), white noise (middle), and colored noise (bottom).

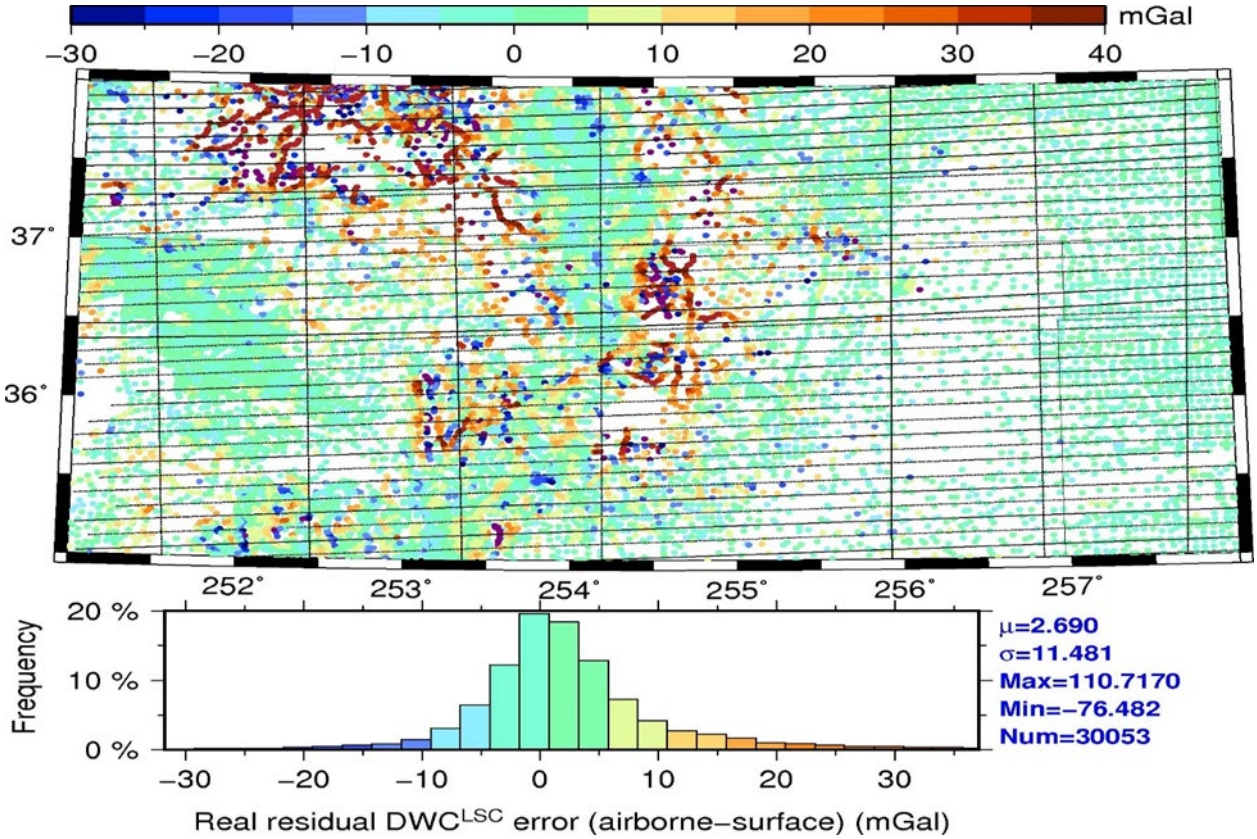

Figure 16. Differences between LSC downward continued residual airborne data and residual surface gravity data. No RTM correction applied.

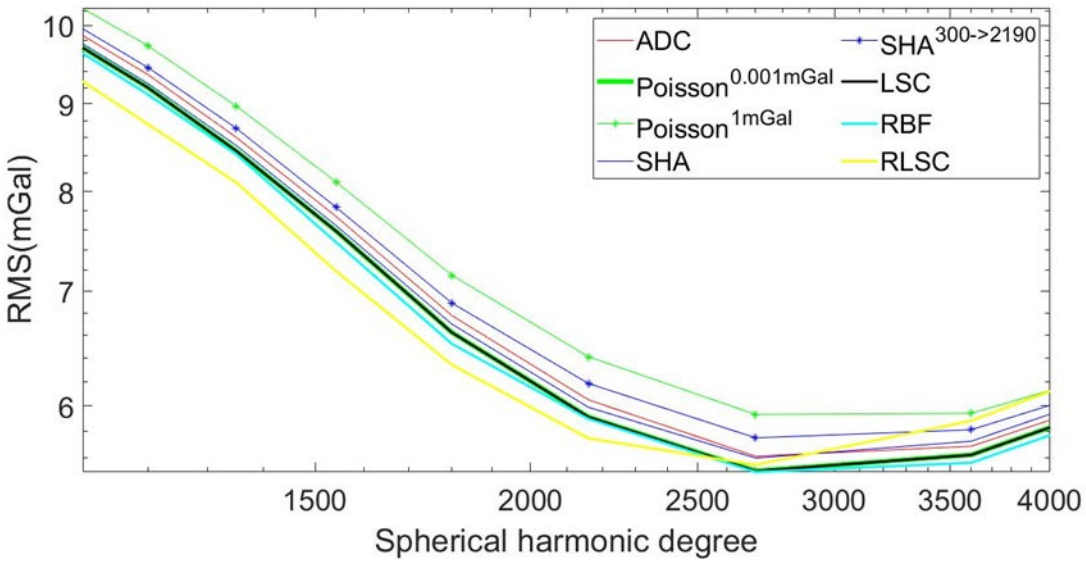

Figure 17. RMS of the differences between the downward continued airborne data and control surface data as function of the reference spherical harmonic degree of the RTM effect removed.

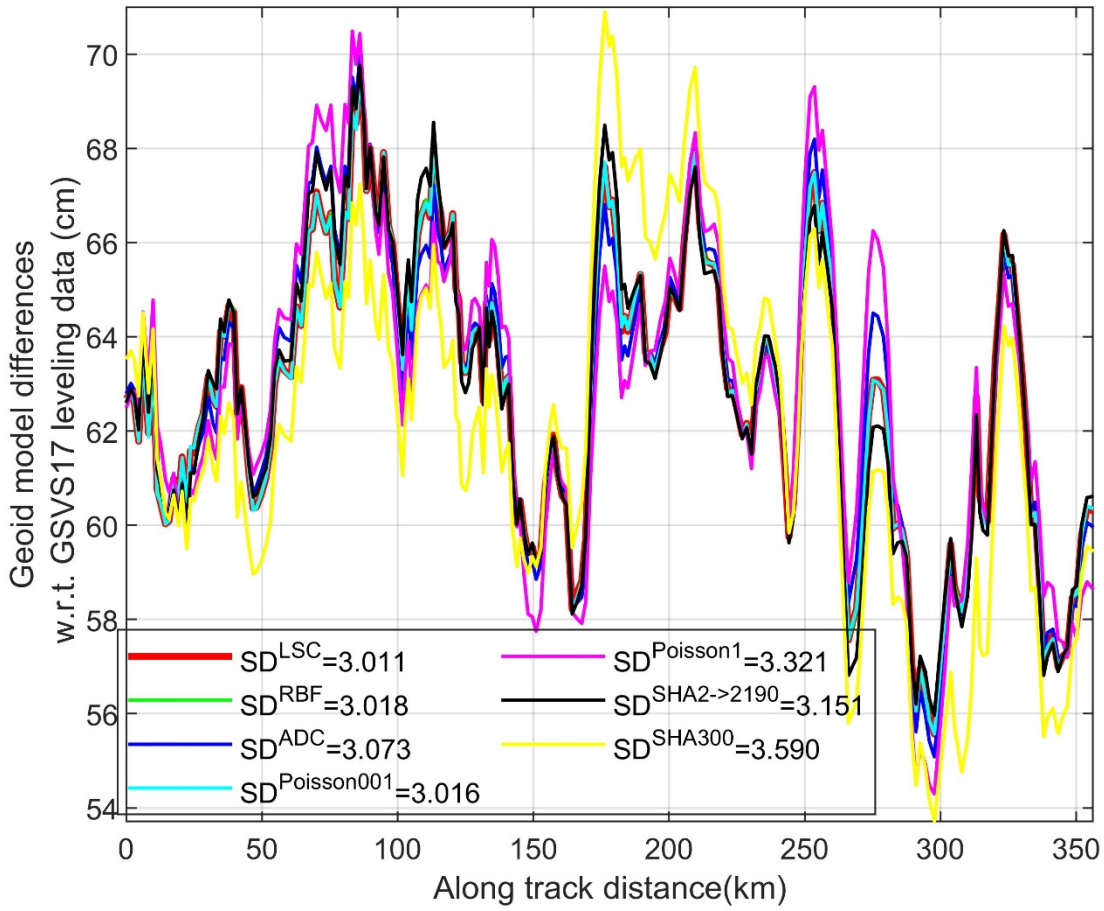

Figure 18. Geoid model differences with respect to the GSVS17 validation data.